SCIENCE CHINA
Technological Sciences

•Article•

July 2018 Vol.61 No.7: 1003–1011
https://doi.org/10.1007/s11431-017-9249-2

Material analysis of the fatigue mechanism of rollers in tapered roller bearings

GUO Wei, CAO HongRui*, ZI YanYang & HE ZhengJia

State Key Laboratory for Manufacturing Systems Engineering, Xi'an Jiaotong University, Xi'an 710049, China

Received May 16, 2017; accepted April 8, 2018; published online May 18, 2018

Rolling contact fatigue is the main failure mechanism of tapered roller bearings. This study investigated the fatigue mechanism of rollers in a tapered roller bearing that failed in a run-to-failure test. Roller microstructure and crack morphology were investigated through scanning electron microscopy. A microhardness test was performed to investigate the strain hardening of the roller material induced by rolling contact fatigue. Results showed that microcavities and holes are important influential factors of crack initiation and propagation. Crack propagation angle affects crack morphology and propagation mode. Material strain hardening accelerates crack growth. Furthermore, roller misalignment causes uneven hardenability and severe damage to roller ends.

rolling contact fatigue mechanism, crack propagation, material microstructure, roller misalignment

Citation: Guo W, Cao H R, Zi Y Y, et al. Material analysis of the fatigue mechanism of rollers in tapered roller bearings. Sci China Tech Sci, 2018, 61: 1003–1011, https://doi.org/10.1007/s11431-017-9249-2

1 Introduction

Tapered rolling bearings have pivotal roles in transmission. They are widely used in machines and railways and in the aerospace and military industries. The failure of tapered rolling bearings not only reduces the usability of mechanical equipment but also causes serious accidents that endanger human safety. Researchers have developed methods based on signal processing and feature extraction for the diagnosis of bearing faults [1–3]. Meanwhile, the study on failure mechanisms and approaches to delay bearing failure from the fault source is extremely rewarding.

Rolling contact fatigue (RCF) is the main form of rolling bearing failure [4]. Many researchers have studied the RCF damage mechanism of rolling bearings. For example, the RCF damage mechanism based on wheel/rail contact mode under different operating conditions has been studied. Raceway surface damage evolution and its behavior in pre-dented hybrid rolling bearings have been observed and modeled [5]. The contact fatigue life of different steels has been identified through an experimental approach for RCF and shelling evaluation based on simulations of the optimal boundary conditions for actual railroad applications [6]. The effects of operational speeds and tangential forces on wear and RCF characteristics, such as surface hardness, shear strain hardening, and wear rate, of wheel materials have been explored [7,8]. The effects of slip ratio on RCF and the wear of wheel/rail materials have been studied via rolling-sliding wear tests [9]. The relationship between RCF cracking after cyclic wheel/rail contact and the plastic deformation of a pearlitic microstructure has been investigated from a microstructural perspective [10,11]. Furthermore, the action mechanisms of material microstructure, grain size, inclusions, holes, and carbides on fatigue damage have attracted considerable attention. The relationship between material fatigue performance and microstructural parameters, such as austenite grain size, martensite width, and carbide and twin crystal distribution, has been discussed [12–14]. The effects

* Corresponding author (email: chr@mail.xjtu.edu.cn)

© Science China Press and Springer-Verlag GmbH Germany 2018

of shapes and sizes of circular hole defects on RCF crack initiation and propagation in high-strength steel has been clarified [15]. The RCF lives of AISI 8620 steel specimens with different retained austenite contents have been calculated through numerical analysis and experimental methods. The results indicated that high austenite content extends RCF lifespan [16]. Moreover, the microstructural variation in the surrounding matrix metal during crack initiation has been quantified. The influence of slippage on rolling contact and wear on a microscopic level has been investigated [17], and a novel vortex-shaped microstructure centered on nonmetallic inclusions near the contact surface has been identified as the crack origin [18]. The mechanism of crack initiation from holes has been revealed [19,20]. However, some studies on crack initiation and crack propagation mechanism have mainly focused on the wheel/rail contact mode but have paid limited attention to the effect of bearing contact mode on fatigue damage. Furthermore, some studies examined the RCF behavior of a certain material through rolling fatigue tests, such as double-disc test and four-ball test, but not the fatigue flaking behavior of bearings under actual operating conditions. Moreover, research on the damage mechanism of rollers of tapered roller bearings is rare, and research on the effects of strain hardening, material defects, and contributing factors on crack initiation and propagation remains insufficient.

In this study, the fatigue crack initiation and propagation mechanism of the rollers of tapered roller bearings were studied through material experiments. The tapered roller bearings were damaged from a run-to-fail test that was performed under actual operating conditions. The relationship between crack propagation angle and crack morphology was studied by analyzing fatigue cracks on roller radial sections. Moreover, microhardness tests were performed to identify the influence of strain hardening on crack initiation and propagation.

2 Material and experimental procedures

Given that the majority of related studies have been conducted on cones and few have been conducted on rollers, this study takes rollers as the research subject. The selected rollers were parts of a failed bearing (30311 tapered roller bearing) collected from a bearing run-to-failure test. The tested bearings in this study were TMB-tapered roller bearings produced by Zhejiang Tianma Bearing Ltd. The bearing run-to-failure test was performed with a T20-60nF fatigue life tester. The running state of the bearings was monitored by a computer connected to the tester. The operating principle is shown in Figure 1. Two testing tapered roller bearings, bearing 1 and bearing 4, were installed on two ends of a shaft. Axial load was directly applied on the cup of bearing 1

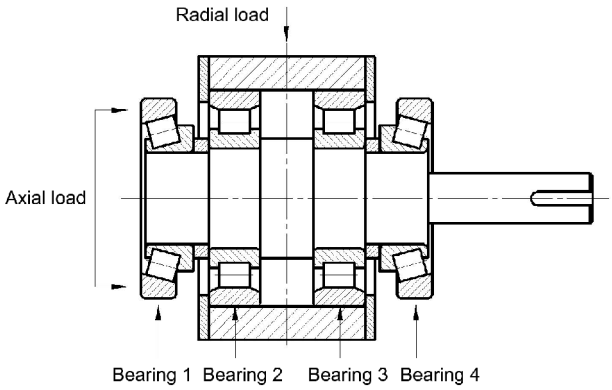

Figure 1 Loading of bearing in the run-to-failure test.

and then transmitted to bearing 4 through the shaft [21]. The run-to-failure test of the tapered roller bearing was performed eight times with different loads and different rotational speeds. In these experiments, fatigue damage appeared on the cup only once, and the majority of the damage was observed on rollers and cones. Test conditions used in this study were 30 kN axial load and 1500 r min^{-1} rotational speed. After 78.5 h, an abnormal signal was observed on the monitor. Figure 2 shows that intensive fatigue damage occurred on the roller surface.

The rollers were made of GCr15 (standard AISI52100). Infrared spectroscopy was performed to clarify the chemical composition of the rollers. Samples were cut as shown in Figure 3. For metallographic observation, the cut samples were embedded in Bakelite, polished, and etched with 4 vol. % Nital. The microstructures of samples of radial sections were observed through scanning electron microscopy (SEM). Axial sections of the samples were subjected to the microhardness test.

3 Results and discussion

3.1 Chemical components of the material

Table 1 shows the chemical composition (in weight percentage) of the roller material and its comparison with the

Figure 2 (Color Online) Fatigue damage on the test roller surface.

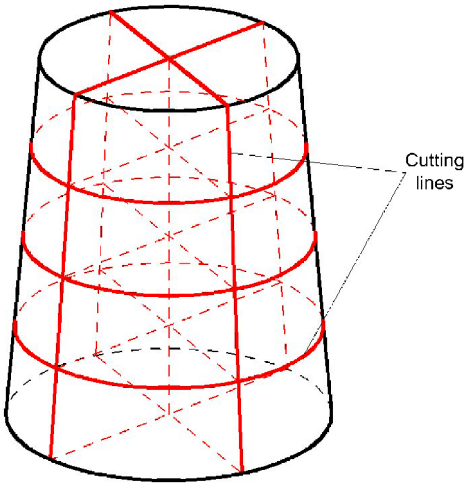

Figure 3 (Color online) Cutting method of samples.

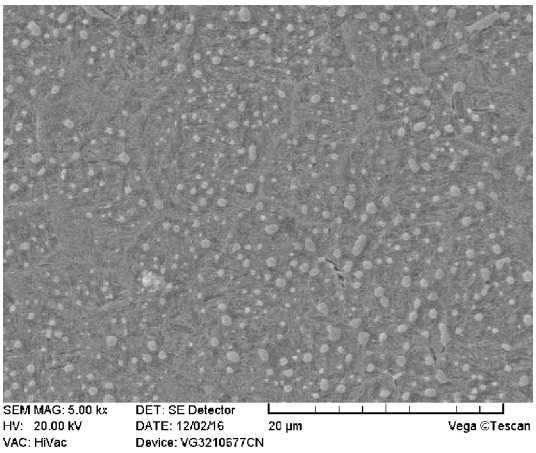

Figure 4 Microstructure of GCr15.

Table 1 Chemical compositions (wt.%) of GCr15

	C	Cr	Si	Mn	S	P
Standard value	0.95–1.05	1.40–1.65	0.15–0.35	0.25–0.45	≤0.025	≤0.025
Estimated value	0.926	1.493	0.255	0.336	0.006	0.017

standard composition of the GCr15. This table shows that the carbon content of the roller material is slightly lower than the standard, whereas the contents of other alloy elements and trace elements are in the normal range. The change in the carbon content of the steel will cause microstructural changes and consequently result in variations in mechanical properties. High carbon contents are associated with high hardness, strength, and abrasive resistance. However, high carbon content is also associated with low plasticity and toughness. The material microstructure of the rollers comprises tempered martensite and spherical carbide, which are uniformly distributed in the matrix structure as shown in Figure 4.

3.2 Appearance of fatigue cracks on roller sections

Crack growth angle, crack length, and crack depth were statistically analyzed as shown in Figure 5. The cracks were distributed over four radial sections with different sizes. In Figure 5, square, circle, triangle and diamond symbols are used to represent the four sections from the large end to the small end of rollers. The figure shows that crack angles mostly fall in the range of 15°–45°. RCF cracks generally grow at an angle of 15°–45° during the inception phase [22]. This behavior indicated that the present experimental results well correspond with the published results. The cracks will then either continue to propagate along a specific direction and gradually approach the roller surface, stop growing, or

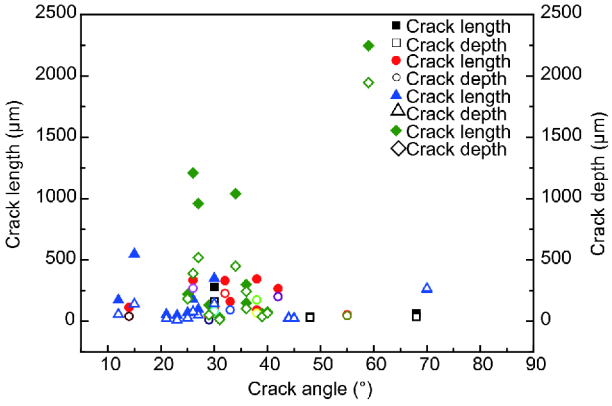

Figure 5 (Color online) Distribution of crack growth angle, crack length, and crack depth.

develop secondary branching cracks. Some of the secondary cracks will grow to the roller surface, whereas others will gradually propagate to the interior of the roller. Crack direction is mainly controlled by two principles: stress criterion and energy criterion. Stress criterion shows that crack propagation along a certain direction is controlled by the maximum stress. Stress criterion may exert a global or local effect on crack propagation. If the stress distribution at the front of the crack changes as a result of crack growth, the direction of the maximum stress at the front of crack may not coincide with the whole direction of the maximum stress. Then, the crack will deviate because it propagates along the direction determined by the local maximum stress. The original crack propagation direction will then change. Cracks may propagate not only along the direction of maximum stress but also along other directions. This phenomenon is attributed to the energy criterion, which states that the crack always grows along the path of least resistance toward regions with the lowest energy. Thus, low-energy regions usually have more material or centralized defects than other regions. Given that the maximum shear stress below the

surface is the driving force of RCF, the Hertzian stress field has an important effect on crack propagation. When the crack grows to the roller surface, it will continue to grow and induce flaking under the influence of the Hertzian stress field. When the crack grows to the roller center, however, it will gradually avoid the effects of the Hertzian stress field and finally stop growing.

Two major fatigue cracks with two modes of crack evolution are observed on the radial sections of the rollers. As shown in Figure 5, numerous long cracks accumulate in regions close to the small end of the roller. Four cracks of up to 1000 μm in size are present in the smallest radial section (diamond-shaped markers). These cracks have different propagation angles. Specifically, three of these cracks have propagated at an angle of approximately 30°, and one has propagated at a large angle of 59°. Cracks with small angles are illustrated in Figure 6. The lengths of the two cracks shown in Figure 6 exceed 1000 μm. These cracks appear torturous and exhibit a number of secondary cracks. The main cracks shown in Figure 6(a) and (b) propagated at an angle of 27° and 26°, respectively. The morphology of these cracks is the most commonly observed among all the observed cracks.

Figure 7(a)–(d) show details of the crack shown in Figure 6 (a) in areas 1–4. Under shear stresses, the main crack propagates primarily in sliding mode (mode II), indicating that

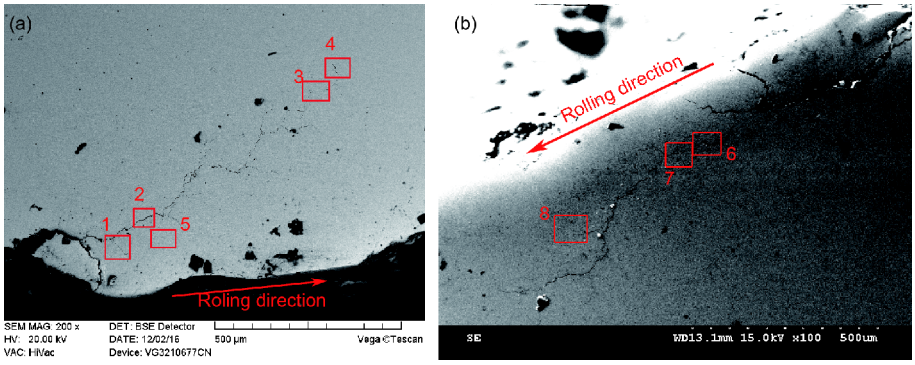

Figure 6 (Color online) Tortuous cracks with some secondary cracks.

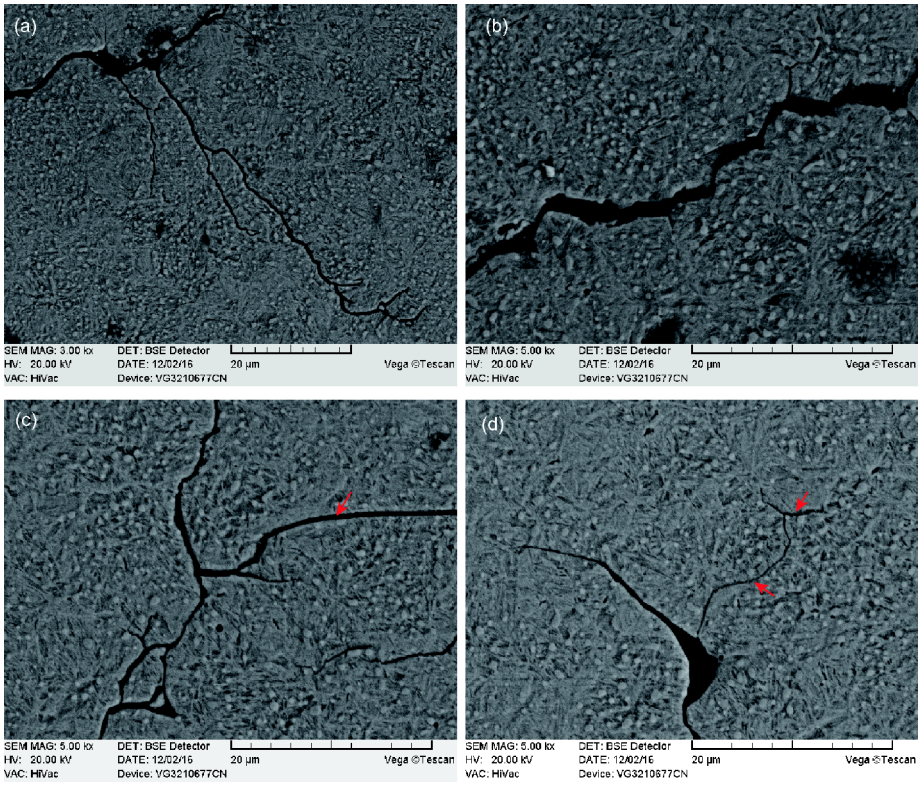

Figure 7 (Color online) Microstructure of the subsurface crack in Figure 6(a).

the cracks mainly formed through edge dislocation gliding. Crack propagation involves a combination of transgranular and intergranular behaviors. The secondary crack shown in Figure 7(a) and the main crack shown in Figure 7(b) exhibit typical tranagranular crack behavior, and the secondary cracks shown in Figure 7(c) and 7(d) present intergranular crack characteristics (arrow). Following the principle of the minimum consumption of fracture energy, cracks always appeared in the weakest points of the material structure and propagated along the slide surface with the weakest bonding. The orientations of martensite layers in the crystalline and the atomic bonding forces of crystal face are different. Under cyclic stress, cracks easily generate on a crystal face with the weakest bonding force. Crack growth in grain boundaries may follow two paths: into another grain or along grain boundaries. Crack propagation is the result of dislocation motion. Given that a mass of dislocations gather on grain boundaries, the combination bond of the grain boundary may not be the weakest. However, if the grain boundary of the material weakens for some reasons, the crack will grow along the grain boundary. Carbide precipitation, which can be observed around the intergranular cracks shown in Figure 7(c) and 7(d) decreases the bond energy of the grain boundary. Thus, intergranular cracks have formed on the grain boundary. As can be seen in the figures, spherical carbides are evenly distributed in the grains. The high hardness of spherical carbides prevents crack penetration. Thus, the cracks stop propagating, continue growing around the spherical carbide, or begin to branch.

For the crack shown in Figure 6(b), the main crack first propagates to the roller surface, and secondary cracks then branch from the main crack and grow into the roller. The secondary branches are very fine. Magnified images of areas 6–8 are shown in Figure 8(a)–(c). The cracks exhibit characteristics of sliding fatigue cracking (mode II), which is driven by shear stress. The crack closure effect has been observed during fatigue crack propagation, and Wolf [23] described the crack closure effect. Crack propagation rate is restricted by the stress status of the crack tip and is influenced by the crack-surface contact region behind the crack tip. Crack closure will impede fatigue crack growth and is affected by oxide effects and material characteristics, such as material plasticity and roughness. Many researchers [24–26] have established models to study this effect and have revised the strength factor of the crack tip.

The subsurface crack shown in Figure 9 is the longest crack among all the observed cracks. It propagates obliquely downwards from the surface spalling with a length of approximately 2246 μm. The angle between the crack growth path and roller surface is approximately 59°. The crack appears straight with a sharp end and lacks secondary branching. The crack follows a microscopic zigzag growth path and has few locally expanding branching cracks. This crack was observed only once on the radial sections. Figure 9 (b) and 9(c) show that similar to the propagation mode discussed above, the crack growth path in the matrix metal exhibits a combination of transgranular and intergranular characteristics. Moreover, the propagation mode of this crack involves not only opening (mode I) or sliding (mode II), but a combination of the two modes. The large propagation angle of the crack indicates that the crack grows in opening mode under shear stress and in sliding mode under compressive stress. Thus, the fatigue crack extends to the roller core over a long distance under alternating stress.

The above three cracks exhibit different propagation characteristics. The fatigue crack with a growth angle of 59° has few secondary cracks, whereas the other two cracks have numerous secondary cracks that branch from the main crack and secondary cracks that grow to the roller surface to form fatigue spallings. Stress intensity factors (SIFs) are key determinants of crack growth behavior. The relationship between crack growth rate and SIFs for various kinds of materials can be calculated using the Paris law [27]:

$$\frac{\mathrm{d}a}{\mathrm{d}N} = C\Delta K_{\mathrm{eq}}^{m}, \tag{1}$$

where a represents crack length, N is the number of loading cycles, ΔK_{eq} is the equivalent SIF range, and C and m are material constants.

Tanaka [28] suggested the equivalent SIF for a mixed-mode crack:

$$\Delta K_{\mathrm{eq}} = \left(\Delta K_{\mathrm{I}}^{4} + 8\Delta K_{\mathrm{II}}^{4}\right)^{1/4}, \tag{2}$$

where ΔK_{I} and ΔK_{II} are the SIF ranges of modes I and II, respectively.

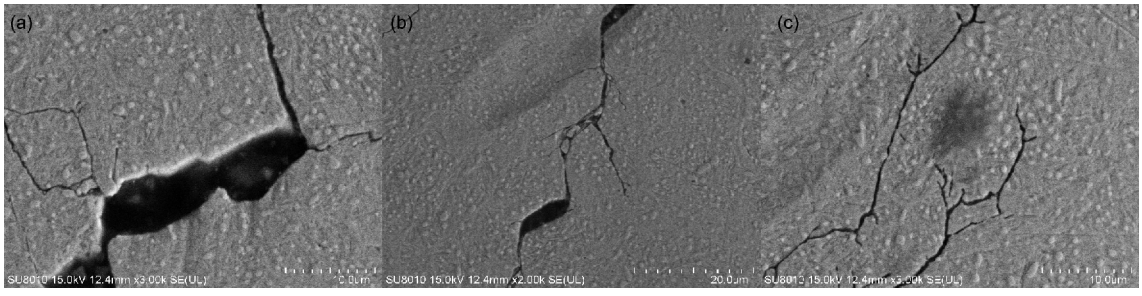

Figure 8 The micro appearance of the subsurface crack in Figure 6(b).

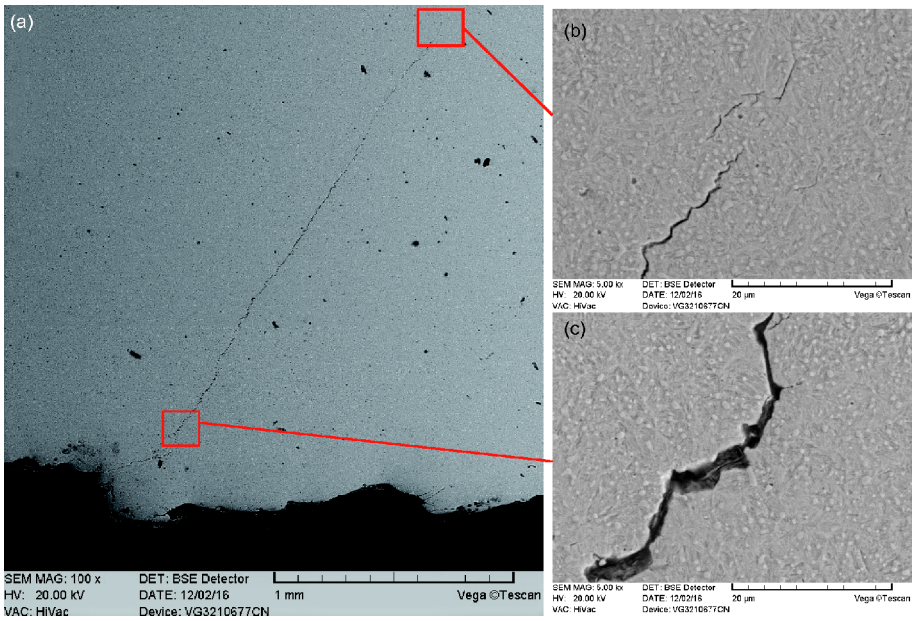

Figure 9 (Color online) Straight crack without any secondary cracks.

From the maximum circumferential stress criterion proposed by Erdogan and Sih [29], the formula describing the relationship between crack growth angle θ and SIFs is as follows:

$$K_{\mathrm{I}}\sin\theta + K_{\mathrm{II}}(3\cos\theta - 1) = 0. \tag{3}$$

Thus, crack growth angle can significantly affect the propagation behavior of a crack with a mixed propagation mode. Cracks with small angles, such as the cracks shown in Figure 6, primarily grow in sliding mode and at shallow depths. Cracks with large angles, such as the cracks shown in Figure 9, are considerably influenced by opening mode. Therefore, the two kinds of cracks shown in Figures 6 and 9 exhibit drastically different crack growth rates and SIFs.

Figures 6–9 show the existence of several holes and microcracks in the matrix metal surrounding the main and secondary cracks. These holes and microcracks tend to act as crack sources and grow into large cracks under alternating stress. Most of the microcracks are generated at the border of spherical carbides given the difference between the material characteristics of the martensite matrix and spherical carbides. Under cyclic stress, the matrix structure exhibits plastic deformation while the spherical carbide remains unchanged. Thus, the joining of the carbide and martensite matrix will cause stress concentration, and the carbide will be stripped from the matrix to form a microcrack. Shiozawa et al. [30] used the carbide stripping model to study carbide stripping under ultra long-life fatigue. At shallow depths, material defects tend to accumulate around small-angle cracks, and numerous secondary cracks tend to form. Small-angle cracks are more likely to develop into fatigue spalling, whereas large-angle cracks are more likely to result in material fracture.

Similar situations are observed for some of the crack tips shown in Figure 10. This figure shows that some microcracks and holes are distributed around cracks. Figure 10(a) shows cracks on an area without any fatigue spalling on the roller surface, and plastic deformation is apparent near the surface. This damage pattern illustrates that under cyclic Hertzian stress, plastic deformation occurs near the roller surface. In crystalline material, stress concentration exists on the front of the dislocation pile-up group caused by localized plastic deformation. Once the concentration of localized stress exceeds fracture strength, the combination bond will be broken, and microcracks will be produced. Crack resistance is closely linked with the localized plastic deformation of the crack tip.

Microcracks will continue to grow under cyclic stress and develop into macrocracks or link with other cracks. The secondary cracks indicated by the black arrows in Figure 10 (b) and (c) are formed by fully developed microcracks that have joined the primary crack. The microcracks indicated by white arrows tend to connect with some other secondary cracks.

Figure 11 shows the microstructures of the central and subsurface regions of the radial section. Figure 11(a) shows the microstructures present in the central region. The images show that fine granular carbides are evenly distributed on the martensitic matrix structure with very few material defects. However, as shown in Figure 11(b), which represents the microstructure of the subsurface of area 5 in Figure 6(a), numerous microcavities and holes are present on the sub-

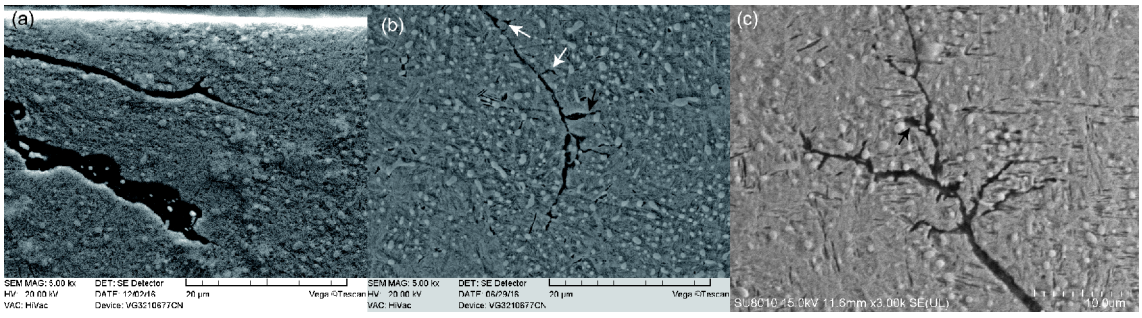

Figure 10 Microstructure of several crack tips surrounded by microcavities.

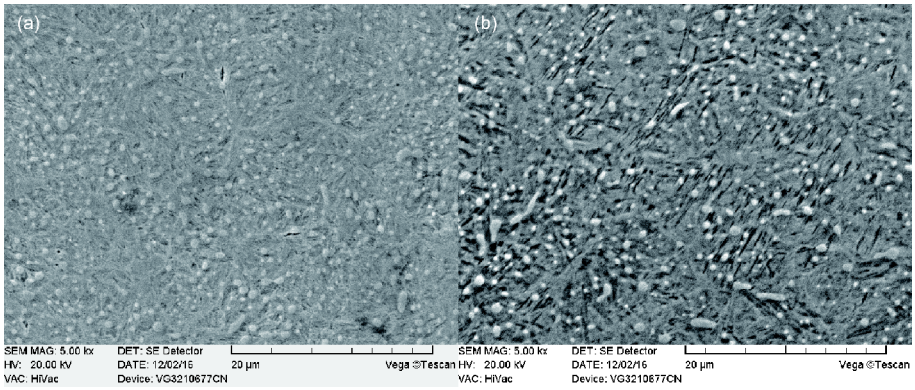

Figure 11 Microstructure of roller matrix material (a) centre structure on the radial section; (b) subsurface structure of detail of area '5' on the radial section.

surface under the rolling contact surface. These material defects are generated from the concentration of plastic strain in the microregion and irreversible dislocation gliding under alternating load. As plastic deformation continues to accumulate, dislocation pile-up results in sufficient stress concentration. When the strain energy released from dislocation movement meets the amount of surface energy required to produce cracks, microcavities and holes will be constantly generated in the subsurface. If the bearing continues working, these microcavities and holes can connect to one another to form microcracks that then finally grow into macrocracks.

3.3 Microhardness analysis of roller

Fatigue flakes are present on the roller surface, as shown in Figure 2. All flakes are concentrated on the small end of the rollers. The microhardness experiment was performed with the MH-5 microhardness system under a load of 300 g and holding time of 15 s. Hardness is measured on the axial section from the roller surface to its center. Five test positions and microhardness change curves are illustrated in Figure 12. The figure shows that the material near the roller surface has hardened after undergoing RCF. When external load is applied on the roller surface, the strain field generated from normal and tangential forces causes the contact surface layer to undergo plastic deformation and increases microhardness [31]. As shown in Figure 12, microhardness decreases when the distance from the surface increases. This behavior, however, varies per position. Microhardness change decreases from position 1 near the large end of the roller to position 5 near the small end of the roller. This behavior indicates that different levels of surface strain hardening occur near the roller surface at different positions of the roller. The strain field under the surface has a certain range. Once depth exceeds this range, strain hardening will stop, thus proving that RCF will no longer affect microhardness at a depth that exceeds the width of the hardening zone. As can be seen in Figure 12, the width of the hardening layer is approximately 1.2 mm. The distribution of the fatigue cracks on the roller sections shown in Figure 5 indicate that cracks propagate under the roller surface at a depth of approximately 600 μm save for the crack shown in Figure 10. Thus, fatigue cracks mostly grow within the range of the hardening layer.

Crack propagation behavior is correlated with the existence of a plastic zone in the crack tip. Numerous studies have attempted to introduce the plastic zone as a mechanical parameter to fatigue failure criterion [32,33]. The plastic zone in the front of the crack can effectively decrease the SIF of the crack tip and thus increase the toughness of the material. Large plastic zones are associated with considerable increases in toughness. The plastic zone size r_p can be ob-

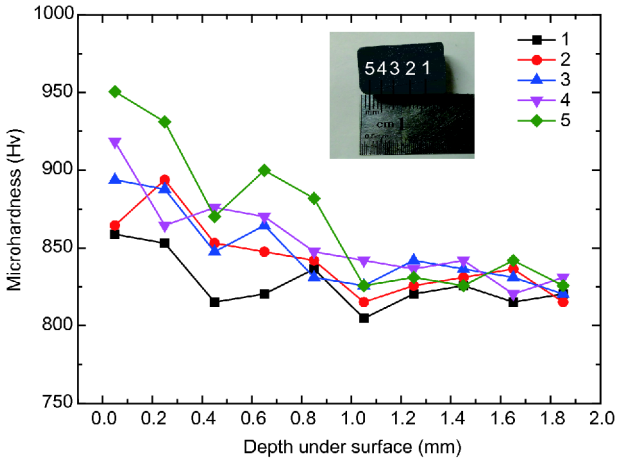

Figure 12 (Color online) Microhardness distribution from contact surface to center on 5 different positions (as shown in insert image) on axial section of a roller.

tained from eq. (4) [34].

$$r_{\mathrm{p}} = \frac{1}{2\sqrt{2}\pi}\left(\frac{K}{\sigma_b}\right)^2, \tag{4}$$

where σ_b is the yield strength.

The modified experiential formula of the plastic zone size of general hardening materials under plane strain conditions is as follows:

$$r_{\mathrm{p}} = \frac{1}{6\pi}\left(\frac{1}{n^2-1}\right)\left(\frac{K}{\sigma_b}\right)^2, \tag{5}$$

where n is the hardening exponent. The formulas indicate that the plastic zone size at the crack tip decreases as the hardening exponent n increases. That is, increasing hardness will accelerate crack growth.

Furthermore, the roller surface subjecting to strain hardening increases material brittleness and decreases fracture toughness. This behavior will promote crack initiation and propagation. Thus, the small end of roller is easily and severely damaged as a result of the strain hardening degree.

Ideally, applied load is evenly distributed over the total length of the roller with crowning designed to counteract edge loading at the roller ends. The width of the hardening layer and the distribution of microhardness at different positions should equal. However, imposing axial load on the bearing may cause roller tilting because of the momentary coupling caused by the opposing axial applied force [4]. Load distribution on the roller will no longer be uniform because of roller tilting, as illustrated in Figure 13. Except for heavy axial load, an assembly problem may result in bearing raceway and roller misalignment and consequently cause uneven loading on the rollers. Furthermore, the roller rotates around the central axis of the bearing at a certain angular velocity and simultaneously rotates around its own axis at high speed. Gyroscopic moment is generated when

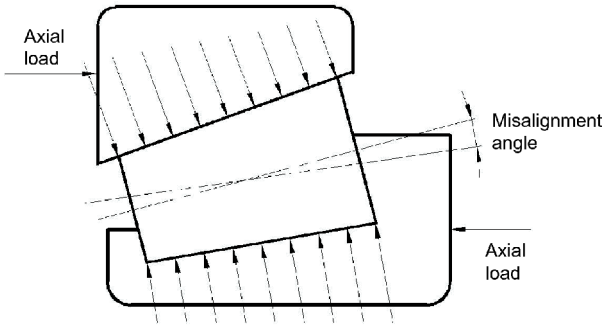

Figure 13 Schematic of uneven load distribution resulting from roller misalignment.

the roller's axis of rotation is tilted with respect to the bearing's axis of revolution. Zhao et al. [35] studied the influences of gyroscopic moment on the damage experienced by a tapered roller bearing and concluded that the boundary conditions produced by gyroscopic moment account for the side damage of rollers and raceways. Uneven loading and gyroscopic moment rapidly increase contact stress on the roller ends. Fatigue flaking will favor the roller end with the constantly running bearing. Under higher applied stress, cracks initiate at the small roller end, and the material hardness of the small roller end will increase. These phenomena have a crucial role in crack growth and new microcrack initiation. Therefore, fatigue damage on the small end of the roller will become severe.

4 Conclusions

To identify the fatigue mechanism and the influential factors of fatigue crack propagation in rollers, rollers were subjected to microstructural and microhardness analyses. The underlying reason for the generation of higher numbers of fatigue spallings at the small end than at the large end of rollers was discussed. The following conclusions are drawn on the basis of the investigation presented above:

(1) Crack growth mode varies because crack angle varies. This variation, in turn, results in the variable degree of fatigue damage experienced by the roller.

(2) Microcavities and holes are key factors of crack initiation and propagation. A large amount of microcavities and holes in the subsurface region will develop into microcracks and finally extend into macrocracks.

(3) Roller misalignment causes stress to concentrate on the small end of the roller, which consequently suffers additional damage.

This work was supported by National Natural Science Foundation of China (Grant No. 51421004) and Key Project supported by National Natural Science Foundation of China (Grant No. 61633001).

1 Jiang L L, Liu Y L, Li X J, et al. Degradation assessment and fault diagnosis for roller bearing based on AR model and fuzzy cluster analysis. Shock Vib, 2011, 18: 127–137
2 Lei Y G, Lin J, He Z J, et al. Application of an improved kurtogram method for fault diagnosis of rolling element bearings. Mech Syst Signal Pr, 2011, 25: 1738–1749
3 Wang W, Lee H. An energy kurtosis demodulation technique for signal denoising and bearing fault detection. Meas Sci Technol, 2013, 24: 025601
4 Harris T A, Kotzalas M N. Essential Concepts of Bearing Technology. 5th ed. Boca Raton: CRC Press, 2006
5 Vieillard C, Kadin Y, Morales-Espejel G E, et al. An experimental and theoretical study of surface rolling contact fatigue damage progression in hybrid bearings with artificial dents. Wear, 2016, 364-365: 211–223
6 Sciammarella C A, Chen R J S, Gallo P, et al. Experimental evaluation of rolling contact fatigue in railroad wheels. Int J Fatigue, 2016, 91: 158–170
7 He C G, Guo J, Liu Q Y, et al. Experimental investigation on the effect of operating speeds on wear and rolling contact fatigue damage of wheel materials. Wear, 2016, 364-365: 257–269
8 He C G, Huang Y B, Ma L, et al. Experimental investigation on the effect of tangential force on wear and rolling contact fatigue behaviors of wheel material. Tribol Int, 2015, 92: 307–316
9 Gui X L, Wang K K, Gao G H, et al. Rolling contact fatigue of bainitic rail steels: The significance of microstructure. Mater Sci Eng-A, 2016, 657: 82–85
10 Benoît D, Salima B, Marion R. Multiscale characterization of head check initiation on rails under rolling contact fatigue: Mechanical and microstructure analysis. Wear, 2016, 366-367: 383–391
11 Ma L, He C G, Zhao X J, et al. Study on wear and rolling contact fatigue behaviors of wheel/rail materials under different slip ratio conditions. Wear, 2016, 366-367: 13–26
12 Tokaji K, Horie T, Enomoto Y. Roles of microstructure and carbides in fatigue crack propagation in high V-Cr-Ni cast irons. J Mater Process Tech, 2007, 190: 81–88
13 Garnham J E, Ding R G, Davis C L. Ductile inclusions in rail, subject to compressive rolling-sliding contact. Wear, 2010, 269: 733–746
14 Donzella G, Faccoli M, Mazzù A, et al. Influence of inclusion content on rolling contact fatigue in a gear steel: Experimental analysis and predictive modelling. Eng Fract Mech, 2011, 78: 2761–2774
15 Makino T, Neishi Y, Shiozawa D, et al. Effect of defect shape on rolling contact fatigue crack initiation and propagation in high strength steel. Int J Fatigue, 2016, 92: 507–516
16 Shen Y, Moghadam S M, Sadeghi F, et al. Effect of retained austenite–Compressive residual stresses on rolling contact fatigue life of carburized AISI 8620 steel. Int J Fatigue, 2015, 75: 135–144
17 Zhou Y, Peng J F, Wang W J, et al. Slippage effect on rolling contact wear and damage behavior of pearlitic steels. Wear, 2016, 362-363: 78–86
18 Zheng C, Lv B, Zhang F, et al. A novel microstructure of carbide-free bainitic medium carbon steel observed during rolling contact fatigue. Scripta Mater, 2016, 114: 13–16
19 Li Y, Kang G, Wang C, et al. Vertical short-crack behavior and its application in rolling contact fatigue. Int J Fatigue, 2006, 28: 804–811
20 Tokaji K, Horie T, Enomoto Y. Effects of microstructure and carbide spheroidization on fatigue behaviour in high V-Cr-Ni cast irons. Int J Fatigue, 2006, 28: 281–288
21 Shen Z J, He Z J, Chen X F, et al. A monotonic degradation assessment index of rolling bearings using fuzzy support vector data description and running time. Sensors, 2012, 12: 10109–10135
22 Bower A F. The influence of crack face friction and trapped fluid on surface initiated rolling contact fatigue cracks. J Tribol, 1988, 110: 704–711
23 Wolf E. Fatigue crack closure under cyclic tension. Eng Fract Mech, 1970, 2: 37–45
24 Suresh S, Zamiski G F, Ritchie D R O. Oxide-induced crack closure: An explanation for near-threshold corrosion fatigue crack growth behavior. Metall Mater Trans A, 1981, 12: 1435–1443
25 Solanki K, Daniewicz S R, Newman Jr. J C. Finite element analysis of plasticity-induced fatigue crack closure: An overview. Eng Fract Mech, 2005, 71: 149–171
26 Hou C Y. Three-dimensional finite element analysis of fatigue crack closure behavior in surface flaws. Int J Fatigue, 2004, 26: 1225–1239
27 Paris P, Erdogan F. A critical analysis of crack propagation laws. J Basic Eng, 1963, 85: 528
28 Tanaka K. Fatigue crack propagation from a crack inclined to the cyclic tensile axis. Eng Fract Mech, 1974, 6: 493–507
29 Erdogan F, Sih G C. On the crack extension in plates under plane loading and transverse shear. J Basic Eng, 1963, 85: 519
30 Shiozawa K, Lu L, Ishihara S. S-N curve characteristics and subsurface crack initiation behaviour in ultra-long life fatigue of a high carbon-chromium bearing steel. Fat Frac Eng Mat Struct, 2001, 24: 781–790
31 Qin X F, Sun D L, Xie L Y, et al. Hardening mechanism of Cr5 backup roll material induced by rolling contact fatigue. Mater Sci Eng-A, 2014, 600: 195–199
32 Wasiluk B, Hoshide T. The fracture process in elastic-plastic materials under biaxial cyclic loading. Int J Fatigue, 2003, 25: 221–229
33 Daily J S, Klingbeil N W. Plastic dissipation in mixed-mode fatigue crack growth along plastically mismatched interfaces. Int J Fatigue, 2006, 28: 1725–1738
34 Irwin G R. Plastic zone near a crack and fracture toughness. In: Proceedings of 7th Sagamore Ordnance Materials Conference. Syracuse: Syracuse University Press, 1960. 63–78
35 Zhao J S, Liu W, Zhang Y, et al. Effects of gyroscopic moment on the damage of a tapered roller bearing. Mechanism Machine Theor, 2013, 69: 185–199